Structure, Vol. 11, 13–19, January, 2003, ©2003 Elsevier Science Ltd. All rights reserved. PII S0969-2126(02)00910-3

How does Radiation Damage in Protein Crystals Depend on X-Ray Dose?

Notes from the Bench

Piotr Sliz,[1] Stephen C. Harrison,[1,3] and Gerd Rosenbaum[2]
[1]Department of Biological Chemistry and Molecular Pharmacology
Howard Hughes Medical Institute
Harvard Medical School
Boston, Massachusetts 02115
[2]Department of Biochemistry
University of Georgia
SER-CAT at the APS
Argonne, Illinois 60439

Summary

Is radiation damage to cryopreserved protein crystals strictly proportional to accumulated dose at the high-flux density of beams from undulators at third-generation synchrotron sources? The answer is "yes," for overall damage to several different kinds of protein crystals at flux densities up to 10^{15} ph/sec/mm^2 (APS beamline 19-ID). We find that, at 12 keV (1 Å wavelength), about ten absorbed photons are sufficient to "kill" a unit cell. As this corresponds to about one elastically scattered photon, each unit cell can contribute only about one photon to total Bragg diffraction. The smallest crystal that can yield a full data set to 3.5 Å resolution has a diameter of about 20 μm (100 Å unit cell).

Introduction

Since its inception, protein crystallography has required an effort to understand and control crystal radiation damage [1–3]. The need to tackle this problem increased when synchrotron radiation was first applied to obtain protein diffraction images [4–6], shifting the upper limit of achievable X-ray flux.

Introduction of the liquid nitrogen freezing technique [7] put the problem temporarily aside, although it was clear that small crystals with large unit cells could readily show progressive damage, despite cryopreservation [8]. Attention to the problem again became acute, as third-generation sources, such as the European Synchrotron Radiation Facility in Grenoble, France, the Advanced Photon Source (APS) in Argonne, IL, and the Super Photon Ring 8 in Hyogo-ken, Japan, capable of exposing crystals to radiation exceeding 10^{15} ph/sec/mm^2, became available to general users. Moreover, because the new phasing methods routinely require collection of very large amounts of data, often from very small crystals, the need for systematic studies of damage versus dose has become particularly important.

Radiation damage is initiated by "primary" interactions between the molecules in the crystal and the beam [9]. Absorbed energy is dissipated in at least two ways: as heat (thermal vibration) and as covalent-bond breakage. The primary damage is dose dependent but generally temperature independent. "Secondary" damage to crystals, which is time and temperature dependent, comes from reactive radicals, generated from polypeptide chain or water molecules by the primary events. The radicals diffuse through protein crystals, causing a cascade of further damage.

Primary damage depends purely on accumulated dose. For crystals examined under conditions in which free radicals can indeed diffuse, secondary damage can depend on time as well as dose, and shorter exposures at higher intensities can provide a way to minimize secondary effects during the actual collection of data. To the extent that cryopreservation prevents free radical diffusion altogether, secondary damage becomes insignificant. Crystal decay should then be proportional to cumulative dose, up to fluxes at which heating rates or related phenomena are too great to control. Preliminary estimates [10] and further more refined calculations (G. Rosenbaum and M. Kazmierczak, personal communication) show that even at the intensities of today's third-generation sources, heat production should not exceed the rate at which cooling can extract it; indeed, for the crystals studied here, the calculated temperature increase is only 6.5 K. This conclusion is consistent with the observation that liquid He cooling does not appear to provide greater protection against radiation damage than liquid N_2 [11], even though heat removal is enhanced (M. Kazmierczak, personal communication). Nonetheless, anecdotal evidence for enhanced damage from a given dose in high-flux beams has led to concerns about optimal use of third-generation sources.

Because of these uncertainties, we decided to check systematically the prediction that damage should simply be proportional to total photon dose, independent of the rate of photon delivery. We report here the results of these studies. Our conclusion is that damage is indeed proportional to dose. With proper detector rates, proper goniometers and exposure timing shutters, and proper cooling, beam attenuation is therefore unnecessary, even at the most intense of present day undulator beamlines. We have also analyzed some of the parameters of progressive damage, in a variety of different kinds of protein crystals. Our concerns here are with overall rates of damage, not with specific local events, such as breakage of disulfide bonds and decarboxylation of acidic side chains, which have been studied by others [12–14]. That is, our interest is optimal strategy for collection of data from crystals of complex structures.

Results—General Experimental Strategy

Intensity Changes

For the experiments reported here, we used crystals of two MHC class I complexes, HLA-A2 with a bound

[3]Correspondence: harrison@crystal.harvard.edu

Key words: protein crystals, radiation damage, synchrotron radiation, X-ray crystallography

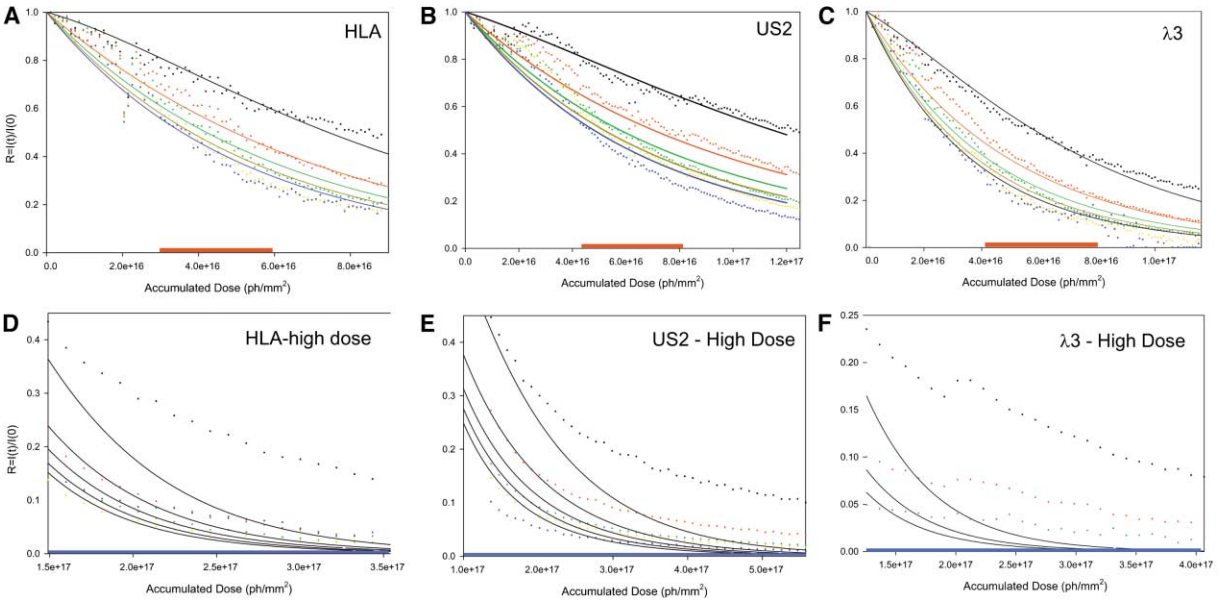

Figure 1. Radiation Damage Factor, I(t)/I(0) Is Plotted against the Accumulated Dose Measured in ph/mm^2 for Reflections Binned in Five Resolution Shells

Panels (A)–(C) represent measurements from batches I–III and (D–F) from batch IV for HLA, US2, and λ3 crystals, respectively. All full and partial reflections are considered. Shell 1 (black line), low resolution (HLA: 30–3.59 Å, US2: 30–4.7 Å, λ3: 30–3.93 Å); shell 2 (red line) (HLA: 3.59–2.85 Å, US2: 4.77–3.79 Å, λ3: 3.93–3.12 Å); shell 3 (green line) (HLA: 2.85–2.49 Å, US2: 3.79–3.32 Å, λ3: 3.12–2.73 Å); shell 4 (yellow line) (HLA: 2.49–2.26 Å, US2: 3.32–3.02 Å, λ3: 2.73–2.48 Å); shell 5 (blue line), (HLA: 2.26–2.1 Å, US2:3.02–2.8 Å, λ3: 2.48–2.3 Å). Frames in batches II are depicted by the red rectangle adjacent to the abscissa.

In preliminary data analysis, the diffracted intensity was evaluated using various criteria, including absolute intensity of full and partial reflections, ratio of intensity to background, and number of reflections with intensities above a certain level. All analyses resulted in similar results, and the graphs presented in Figure 1 are representative of other evaluations. Unexpected jumps in intensity present at frame 21 of the HLA data, at frames 1–20 of the US2 data and frame 110 of λ3 data can probably be attributed to fluctuations in beam intensity. Due to an experimental oversight, the recorded beam intensities for the high-dose rate frames were oversaturated, and therefore the global correction cannot be applied.

melanoma decamer peptide [15] and the ternary US2/HLA-A2/Tax peptide complex [16], as well as crystals of a viral polymerase λ3 from reovirus [17]. We refer to these as HLA, US2, and λ3, respectively. Additional measurement on crystals of a BTB domain [18] and of HIV-1 reverse transcriptase [19] gave similar results.

Our overall approach was straightforward. We collected four batches of 30–40 data frames from a fixed region of each crystal. For each frame, the samples were rotated by 1° during the exposure and then returned to the starting position before the next exposure. The temperature of the samples was maintained at 100 K. At this temperature, there should be essentially no secondary damage unless cooling is insufficient. The dose per frame in batches I–III was kept constant. Frames in batches I and III were collected at low-flux density (aluminum filter used for 10-fold attenuation of the X-ray beam, 5 s exposures), and frames in batch II were collected at high-flux density (removed aluminum filter and exposure time decreased to 0.5 s). The dose per frame in batch IV was increased by a factor of ten (no filter, 5 s exposures). To minimize the possibility of initial damage, the first batch in each run was collected at low-flux density. We then measured the integrated intensities of the reflections on each frame using standard methods and analyzed the data by examining a variety of parameters (unit cell changes, total Bragg intensity changes, R factor changes) as a function of cumulative dose. The crystals were kept in the same orientation, so that observed changes in the diffraction pattern should be functions only of damage and not of different samplings of reciprocal space. We report results for three different crystal types (see Tables 1 and 2).

We observed a significant time-dependent decrease in diffracted intensity in our experiment, which we attribute to radiation damage. Although the intensity is also a function of crystal orientation and of the crystal volume illuminated by the X-ray beam, both variables were eliminated in our experiment by keeping the orientation of crystals constant. The radiation damage factor, I(t)/I(0),

Table 1. Parameters from Equation 1

Data Set	k_1 ((ph/mm^2)$^{-1}$)	k_2 ((ph/mm^2)$^{-1}$)	D(A^2)	Goodness of Fit, R_2
HLA	$2.37 \times 10^{-17} \pm 1.6 \times 10^{-18}$	$1.64 \times 10^{-17} \pm 7.8 \times 10^{-19}$	41.2 ± 4.5	0.957
US2	$1.79 \times 10^{-17} \pm 8.8 \times 10^{-19}$	$8.84 \times 10^{-18} \pm 3.1 \times 10^{-19}$	60.0 ± 5.0	0.953
λ3	$3.10 \times 10^{-17} \pm 1.2 \times 10^{-18}$	$1.88 \times 10^{-17} \pm 5.1 \times 10^{-19}$	50.5 ± 4.0	0.975

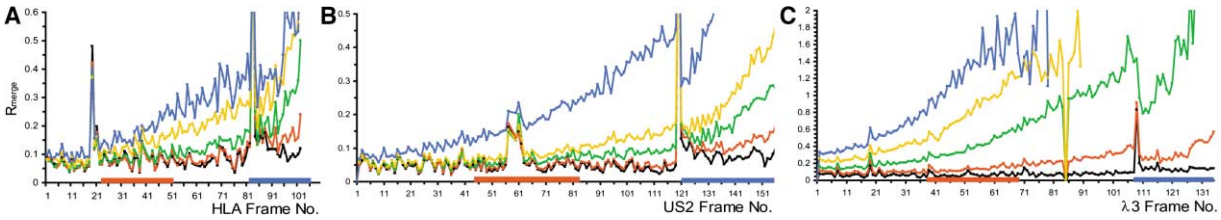

Figure 2. R_{merge} Calculated between First and Any Subsequent Frame and Plotted in Five Resolution Shells for HLA, US2, and λ3 Crystals

(A) HLA, (B) US2, (C) λ3. All full and partial reflections are considered. For limits of resolution shells, see caption to Figure 1. Frames in batches II and IV are depicted by the red and blue rectangles adjacent to the abscissa. The R_{merge} for the high-resolution reflection in batches I–III can be fit uniformly as an exponential increase with coefficient of determination (R^2) of 0.80, 0.97, and 0.96 for HLA, US2, and λ3 crystals, respectively.

where I(t) is the diffracted intensity after exposure t and I(0) is the initial intensity, I(0), calculated from the average intensities diffracted from each of the three crystals, is presented in Figure 1. We observe that I(t)/I(0) decreases uniformly with exposure, and the rate of decay does not change as flux densities alternate from low to high (batches I and III versus batch II). We conclude that radiation damage is independent of flux density.

Blake and Phillips suggest the following model for radiation damage [3]:

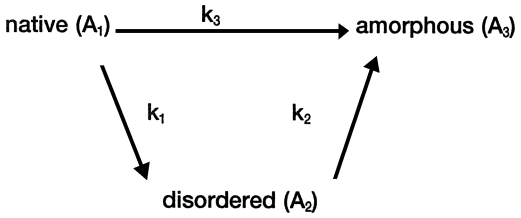

The "disordered" unit cells have elevated temperature factors; the amorphous regions do not give Bragg diffraction at all. Hendrickson [21] showed that this kinetic scheme yields expression (1) for the radiation-damage factor,

$$\frac{I(t)}{I_0} = \exp[-(k_1 + k_3)t] + \frac{k_1}{k_1 + k_3 - k_2}\exp(-k_2 t)$$

$$\{1 - \exp[-(k_1 + k_3 - k_2)t]\}\exp\left(-D\frac{\sin^2\theta}{\lambda^2}\right), \qquad (1)$$

where D measures mean square displacement of atomic positions. In the cases of myoglobin [21], using data collected at room temperature, it was concluded that $k_3 \approx 0$ and that the process of radiation damage is a sequential one. The molecular structure is first disordered by one event or set of events and then effectively denatured by a second. We used simplex and regular nonlinear curve fitting in Origin 7 (OriginLab Corporation) to fit data from batches I–III with expression (1); in all cases the value of k_3 refined to 0 within the experimental error and all other parameters are presented in Table 1. We find that the Blake and Phillips radiation damage model fits our data rather well, even at high-damage dosage (last frame of batch III: 62%, 70%, and 74% overall damage for HLA, US2, and λ3, respectively), although in the high-resolution shells the damage is underestimated by roughly 5%. For crystals at room temperature, the discrepancy at high doses was significantly higher [21]. As suggested by Hendrickson, the discrepancy is expected because once a high proportion of unit cells have been damaged, neighboring cells will be disrupted by local disintegration of the crystal lattice. In the frozen crystals studied in our experiment, such disintegration should be limited until damage is extensive [22, 23].

For frames in batch IV, as crystals absorbed the even higher dose per frame, the radiation damage exceeded 90%. The initial frames of batch IV can still be described by the Blake and Phillips model parameterized using batches I–III, but eventually at the extreme damage the model overestimates the drop in radiation damage factor (Figures 1D–1F). Thus, the 10-fold increase in X-ray dose per frame resulted in 10-fold increase in crystal damage, further demonstrating that radiation damage is strictly proportional to the dose of the absorbed X-rays.

The model for radiation damage embodied in (1) is characterized by four parameters: D, k_1, k_2, and k_3. The values of D for the proteins studied here (Table 1) are in line with numbers obtained for phosphorylase (D between 50 and 100 Å^2) and myoglobin (D between 30 and 70 Å^2). Our estimate of $k_3 \approx 0$ is in line with previously published room temperature data [2, 21], but absolute values of k_1 and k_2 cannot be compared, as they are calculated in different units (ph/mm^2 here versus hours of data collection for room temperature crystals). Nevertheless, consistent with experiments at room temperature, values of k_1 are similar for all three proteins we studied and are comparable to the corresponding values of k_2.

R_{merge} Changes

Analysis of R_{merge} reveals that it is also dose dependent and flux-density independent. The overall R_{merge} gradually increases in all samples studied, but while the increase of the R_{merge} in the higher resolution shells is significant, the R_{merge} for the low-resolution shell remains unchanged (Figure 2). The R_{merge} for the high-resolution reflections in batches I–III can be fit uniformly as an exponential increase, confirming that the radiation damage is independent of flux density. The uniform fit is also true for the high-dose frames in batch IV, although as the intensities are being measured more accurately with higher flux X-rays, the R_{merge} in high-resolution shells at the beginning of batch IV is lower than in the final

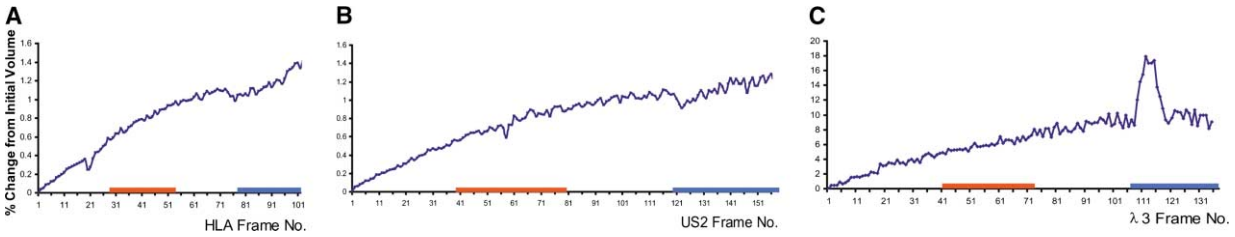

Figure 3. Unit Cell Volume Changes for HLA, US2, and λ3 Crystals

(A) HLA, (B) US2, and (C) λ3. Frames in batches II and IV are shown respectively by the red and blue rectangles adjacent to the abscissa. Analysis of positional errors reveals that they steadily increase in batches I–III (data not shown). This steady increase is probably due to the increasing mosaicity (estimated from Denzo profiles, results not shown) and decreasing number of spots, as weak spots are eliminated by radiation damage. The results for batch IV are not reliable; the positional errors in refinement are too high, as they rapidly jump at the first frame of this batch. The rapid jump in error could be attributed to the increased number of overloads that are excluded from positional refinement (in case of US2 from 18 at frame 119–185 at frame 120).

frames of batch III (Figure 2). The gradual increase in the R_{merge} observed in batches I–III and again in batch IV is not due solely to decreased diffraction intensity (and hence poorer counting statistics). Other factors, specifically structural changes at the atomic level, must have a role. To confirm this hypothesis, we have separately scaled two remote batches of US2 frames, #1–10 and #110–119, and then scaled them together. Statistics for the first batch were excellent, with an overall R factor of 2%. The scaling of the second batch also provided very good statistics with slightly elevated overall R factor, 3.0% for all reflections. The highest resolution shell had significantly deteriorated, as expected, with an R factor of 24.4%, increased from 3.8% for the first batch. The statistics for the two batches scaled together were significantly worse, with an overall R factor of 12%, showing that real structural changes had occurred.

Unit Cell Changes

It has been observed that the exposure of protein crystals to synchrotron radiation causes an increase in unit cell volume [12, 14, 24]. Measured up to a dose of 55×10^{15} ph/mm^2, the effect seems to be linear [14]. In our experiment with a maximum dose of 330×10^{15} ph/mm^2, received by the US2 sample, we observed some leveling off of the unit cell increase (Figure 3), but our method of measuring unit cell parameters was not ideal. Measurement of unit cell axis is linked to other parameters such as crystal detector distance, beam center, and positional errors in the refinement. Accurate, independent estimate of all parameters is difficult if only a single, small angle oscillation is used. The ϕ-χ method [25] would be a better choice to estimate unit cell axes reliably, but it would require several oscillations for each data point, and hence could not be utilized in our setup. The increase in the unit cell dimensions appears to be uniform, and we show that it is independent of the flux density of the beam. We can fit the changes in unit cell volume by the expression $y = y_0 \times A_1 e^{-x/t_1}$, where the rate constant is uniform across groups of exposures at different dose rates. The unit cell expansion is close to 1% for the HLA and US2 crystals but significantly larger for the λ3 crystals (10% at the end of batch III). The higher rate of unit cell expansion in the λ3 crystals is consistent with increased radiation damage determined by changes in R_{merge}.

Discussion

Minimum Crystal Sizes

None of the parameters of damage we have measured depend on flux density. Moreover, we can fit the decline of intensity in Bragg reflections by a four-parameter model (with one parameter, k_3, equal to zero). The model is a highly idealized one, but it is only the rough values of the rate constants that matter for the discussion below. We now ask how the rates of damage we observe limit achievable resolution for a crystal of any chosen size. We proceed as follows. We describe the crystal as "dead" when Bragg intensities at a chosen resolution have fallen to (1/e) of their initial values. We then use the damage versus dose information summarized by the parameters in Table 1 to determine how many photons (on average) can be absorbed by a crystal before it "dies," and we further calculate (using the ratio of elastically scattered to absorbed photons) how many photons have been scattered into Bragg reflections when this point has been reached. The size of the unit cell, and thus the reciprocal-lattice spacing, determines the number of reflections over which these photons are distributed and hence the approximate accuracy with which their intensities can be measured.

We first note that for all the crystals we examined, D in expression (1) is approximately 50 Å^2. This parameter measures the enhanced intensity fall-off with resolution for the "disordered" state. A value of 50 Å^2 corresponds to an attenuation of intensity in Bragg peaks by (1/e) at a spacing of about 3.5 Å. Measurable diffraction at this spacing and beyond will therefore come largely from unit cells in the "native" state. We take as a rule-of-thumb limit for data collection from a given crystal the radiation dose for which the fraction of unit cells in the "native" state has declined to (1/e). This dose is equal to $1/k_1$, or approximately 0.5×10^{17} ph/mm^2. We declare a crystal "dead" when this dose has been reached. In our experiments, with an incident flux density of about 2×10^{15} ph/sec/mm^2, "death" would have occurred at about 25 s total exposure at full intensity, or about 50 frames, as can also be seen by inspection of Figure 1.

Assume that we have crystals of typical dimension d (mm) and average unit cell dimension a (Å). There are $(d/a)^3 \times 10^{21}$ unit cells in such a crystal. The linear absorption coefficient is 0.2 mm^{-1}, so the total dose per

Table 2. Crystals Parameters and Data Collection Strategy

Protein Name, MW of Protomer, Number of Protomers in the Asymmetric Unit, Solvent Content, Crystal Size	Space Group; Initial Unit Cell Dimensions: a, b, c [Å]; α, β, γ [°]	Initial Resolution Limit, Initial Mosaicity	Frame Numbers in Batches I, II, III, and IV
HLA, 48.5 kDa, 1, 45.5%, 0.15 × 0.15 × 0.04 mm^3	$P2_12_12_1$; 49.28, 74.79, 122.74; 90, 90, 90	2.1 Å, 0.20°	1–27, 28–54, 55–81, 82–102
US2, 55.9 kDa, 4, 61%, 0.1 × 0.1 × 0.06 mm^3	P1; 95.92, 100.135, 97.06; 110.10, 108.13, 108.79	2.8 Å, 0.45°	1–39, 40–79, 80–119, 120–155
λ3, 142.3 kDa, 1, 50%, 0.3 × 0.3 × 0.02 mm^3	$P2_12_12_1$; 70.98, 86.44, 247.75; 90, 90, 90	2.3 Å, 0.80°	1–36, 37–72, 73–108, 109–135

unit time absorbed in the crystal is about $(0.2\ \mathrm{mm}^{-1}\ d^3)I_o$. We thus calculate that after 25 s at 2×10^{15} ph/sec/mm^2, each unit cell will have absorbed $a^3 \times 10^{-5}$ photons. The crystals we studied all had $a \approx 100$ Å, so that about 10 absorbed photons were sufficient to "kill" a unit cell. This would seem to be a suitable general estimate: about 10 bond-breaking events might reasonably be expected to disorder a unit cell substantially, although structural details could plausibly produce variations by factors of 2 to 5. Indeed, the damage rate for most "frozen" protein crystals falls within a moderately narrow range [26]. For 12 keV radiation ($\lambda = 1$ Å), each elastically scattered photon corresponds to about 10 absorbed photons [9]. Thus, with the sorts of crystals we have studied and probably with most protein crystals, a unit cell dies after it has contributed on average one photon to total Bragg scattering.

If we rotate a crystal through 180°, to collect a full dataset, it will diffract during this rotation a total of approximately $4(a/\lambda)^3$ reflections, although of course not all of these will be recorded with a conventional detector. Let N be the total number of photons in all the diffracted beams; the average number of photons per Bragg reflection, n, will then be $N/(4(a/\lambda)^3)$. For $n = 1000$ (roughly 3% statistical accuracy on average, although the intensities of the recorded reflections will of course be stronger than this average, since our calculation includes all weak back-scattered reflections, which are not recorded), $N = 4000(a/\lambda)^3$. But for $\lambda = 1$ Å, N is also the total number of units cells needed to diffract this number of photons according to the damage model outlined above. Setting $N = (d/a)^3 \times 10^{21}$, we find that $d_{min} = 1.6 \times 10^{-6}\ a^2$ (d in mm; a in Å) for the size of a crystal required to yield a reasonable 3.5 Å resolution dataset. For $a \approx 100$, $d_{min} \approx 20$ μm. Crystals of the kind we have studied smaller than about 20 μm cannot be expected to yield full data sets. Teng et al. [23] and Glaeser et al. [27] have arrived at similar estimates with measurements using lysozyme and bacteriorhodopsin crystals and beams with a flux density 10^{-3} to 10^{-4} times the one we have used. They calculate the minimum crystal size required for full dataset collection to 35 and 30 μm, respectively, but their resolution criteria are stricter.

An important application of undulator sources will be for recording diffraction from very small crystals. There are various strategies for using an intense but extremely well collimated incident beam to optimize diffracted signal over diffuse background. It may therefore be possible to approach the limits set by the physics of absorption and damage as measured here and to record essentially complete data sets from crystals 10–20 μm in diameter. The quadratic dependence of d_{min} on the unit cell dimension suggests that for unit cells much larger than 100 Å, substantially larger crystals may be required. Large protein complexes, such as ribosomes, may in practice be able to absorb more than 10 photons before disordering completely, and the dependence of minimum crystal size on unit cell size may not (for the kinds of structures that crystallize with very large unit cells) be quite as steep as the quadratic expression suggests. There is, in any case, considerable room for improvement of recording geometries before the damage limits are reached.

Optimal Data Collection Strategies

Our demonstration, that radiation damage in "frozen" crystals is simply proportional to total dose, has consequences for strategies of data collection. As illustrated in the preceding section, there is clearly a trade-off between accuracy of intensity measurements (counting statistics) and the number of measurable reflections (completeness) at a chosen resolution. For collecting "good" data sets at 2.5–3 Å resolution, the typical limit for moderately challenging crystals and new structures, it would be reasonable to record an average of 1000–3000 photons per reflection above background in the region between 6 Å and the outer limit. The weakest terms will have low precision, but the advantage of a relatively complete data set from an undamaged crystal will generally outweigh the improved counting statistics for weak reflections. Within the "water ring," however, between spacings of 4 and 3.5 Å (approximately), diffuse scatter often dominates. The accuracy of weak reflections will be set by the counting statistics of the background, and, if the beam passes through scattering matter outside the crystal itself (ice, oil, etc.) or if the solvent content of the unit cell is high, it may be necessary to overexpose (as judged by the criteria just mentioned) in order to obtain adequate measurements of a reasonable fraction of the recorded data. Reducing the strength of the water ring, relative to that of the Bragg diffraction, by suitable collimation is clearly important.

In those cases for which the goal is to wring the highest possible resolution from crystals with moderate fall off, low-resolution reflections will naturally be vastly overexposed. For example, if the average atomic B is 10 Å^2 for a well-ordered structure, then the mean intensity for reflections at 2 Å resolution is 10-fold greater than the mean intensity at 1.2 Å resolution. To record those 1.2 Å terms with an average of 1000 photons per reflection, data at 2 Å resolution will have an average of 10,000 photons per reflection, and the fraction of

reciprocal space that can be recorded, before the crystal "dies," will be correspondingly reduced.

Whatever the goal, it is useful to be able to estimate photon counts in order to optimize data recording strategies. The relationship between detector or primary beam monitor readings and actual photon counts depends on a variety of installation-dependent factors. Managers of beamlines can make rough calibrations and advise users of suitable ranges.

Experimental Procedures

Crystals

Complete descriptions of crystallization and cryo-protection conditions for HLA, US2, and λ3 can be found in the references cited above and also in see the Supplementary Material available with this article online.

Beamline Setup

Damage studies reported here were performed at beamline 19-ID of the Structural Biology Center at the APS. For details of the storage ring and beamline design, see the Supplementary Material available with this article online. The experiments were performed at an X-ray photon energy of 12.0 keV (wavelength = 1.03 Å).

The radiation dose deposited on the crystal, i.e., energy absorbed per unit mass, is proportional to the flux density on the sample crystals. In order to obtain the highest possible flux density for the damage studies, the beamline was carefully aligned, and the focusing elements were adjusted for the smallest focus on the sample. In order to reduce possible effects of sample heating, the collimator slits were set to cut the tails of the flux density distribution in the horizontal direction decreasing the total flux on the sample while maintaining the flux density in the center. In the vertical direction, the collimator slits were set wider than the height of the beam in order to allow for small beam motions which might occur during the experiment. The focal sizes measured (scanning a 0.012 mm wide slit) were 0.107 mm full-width at half-maximum (FWHM) horizontal and 0.026 mm FWHM vertical (after deconvolution). The collimator slits were set to a width of 0.089 mm and a height of 0.049 mm. The integral flux through the collimator slits was measured with an ion chamber as 3.2×10^{12} ph/s, normalized to 100 mA beam current in the storage ring. With the collimator slits set, the beam size measured was 0.065 mm FWHM × 0.020 mm FWHM, horizontal × vertical, smaller than any of the crystals we examined. The (calculated) peak flux density in the center of the beam was about 2.2×10^{15} ph/s/mm^2/100 mA. The beam current for the measurements reported here was between 70 mA and 100 mA.

Integrated Intensities

The first frame of each data set was indexed, refined, and integrated, and the initial mosaicity was estimated from the mosaicity histogram in Denzo [20] (Table 2). All remaining data frames were subsequently processed using the refined parameters from the first frame as a starting point for each integration. The spot size was set to 0.30 × 0.30 mm and background to 0.40 × 0.40 mm. In batches I–III the established mosaicity was increased for each subsequent frame by 0.001°, and in batch IV, by 0.010°.

The refined unit cell parameters for each frame were extracted from the Denzo log file. The integrated reflections listed in the Denzo x files were analyzed for intensity and R factor using our own script, written in perl.

Supplementary Material

Supplementary Material including additional Experimental Procedures can be found online at http://images.cellpress.com/supmat/supmatin.htm.

Acknowledgments

We thank R. Gaudet, Y. Tao, G. Prive, B. Gewurz, A. Haykov, S. Di Marco, and K. Ahmad for providing crystals for our experiments. Use of the Argonne National Laboratory SBC-CAT beamline at the APS was supported by the U.S. Department of Energy, Basic Energy Sciences, Office of Research, under contract No. W-31-109-Eng-38. S.C.H is an investigator and P.S. is an associate of the Howard Hughes Medical Institute.

Received: July 30, 2002
Revised: October 7, 2002
Accepted: October 11, 2002

References

1. Hendrickson, W.A., Love, W.E., and Karle, J. (1973). Crystal structure analysis of sea lamprey hemoglobin at 2 angstrom resolution. J. Mol. Biol. *74*, 331–361.
2. Fletterick, R.J., Sygusch, J., Murray, N., and Madsen, N.B. (1976). Low-resolution structure of the glycogen phosphorylase alpha monomer and comparison with phosphorylase beta. J. Mol. Biol. *103*, 1–13.
3. Blake, C.C., and Phillips, D.C. (1962). Effects of X-irradiation on single crystals of myoglobin. In Biological Effects of Ionizing Radiation at the Molecular Level (Vienna: International Atomic Energy Agency), pp. 183–191.
4. Rosenbaum, G., Holmes, K.C., and Witz, J. (1971). Synchrotron radiation as a source for X-ray diffraction. Nature *230*, 434–437.
5. Harmsen, A., Leberman, R., and Schulz, G.E. (1976). Comparison of protein crystal diffraction patterns and absolute intensities from synchrotron and conventional x-ray sources. J. Mol. Biol. *104*, 311–314.
6. Phillips, J.C., Wlodawer, A., Yevitz, M.M., and Hodgson, K.O. (1976). Applications of synchrotron radiation to protein crystallography: preliminary results. Proc. Natl. Acad. Sci. USA *73*, 128–132.
7. Hope, H. (1988). Cryocrystallography of biological macromolecules: a generally applicable method. Acta Crystallogr. B *44*, 22–26.
8. Walsh, M.A., Dementieva, I., Evans, G., Sanishvili, R., and Joachimiak, A. (1999). Taking MAD to the extreme: ultrafast protein structure determination. Acta Crystallogr. D *55*, 1168–1173.
9. Henderson, R. (1995). The potential and limitations of neutrons, electrons and X-rays for atomic resolution microscopy of unstained biological molecules. Q. Rev. Biophys. *28*, 171–193.
10. Kuzay, T.M., Kazmierczak, M., and Hsieh, B.J. (2001). X-ray beam/biomaterial thermal interactions in third-generation synchrotron sources. Acta Crystallogr. D *57*, 69–81.
11. Teng, T.-Y., and Moffat, K. (2002). Radiation damage of protein crystals at cryogenic temperatures between 40K and 150K. J. Synchrotron Radiat. *9*, 198–201.
12. Ravelli, R.B., and McSweeney, S.M. (2000). The "fingerprint" that X-rays can leave on structures. Structure *8*, 315–328.
13. Weik, M., Ravelli, R.B., Kryger, G., McSweeney, S., Raves, M.L., Harel, M., Gros, P., Silman, I., Kroon, J., and Sussman, J.L. (2000). Specific chemical and structural damage to proteins produced by synchrotron radiation. Proc. Natl. Acad. Sci. USA *97*, 623–628.
14. Burmeister, W.P. (2000). Structural changes in a cryo-cooled protein crystal owing to radiation damage. Acta Crystallogr. D *56*, 328–341.
15. Sliz, P., Michielin, O., Cerottini, J.C., Luescher, I., Romero, P., Karplus, M., and Wiley, D.C. (2001). Crystal structures of two closely related but antigenically distinct HLA-A2/melanocyte-melanoma tumor-antigen peptide complexes. J. Immunol. *167*, 3276–3284.
16. Gewurz, B.E., Gaudet, R., Tortorella, D., Wang, E.W., Ploegh, H.L., and Wiley, D.C. (2001). Antigen presentation subverted: structure of the human cytomegalovirus protein US2 bound to the class I molecule HLA-A2. Proc. Natl. Acad. Sci. USA *98*, 6794–6799.
17. Tao, Y., Farsetta, D.L., Nibert, M.L., and Harrison, S.C. (2002). RNA synthesis in a cage—structural studies of reovirus polymerase lambda3. Cell *111*, 733–745.
18. Ahmad, K.F., Engel, C.K., and Prive, G.G. (1998). Crystal struc-

ture of the BTB domain from PLZF. Proc. Natl. Acad. Sci. USA *95*, 12123–12128.

19. Rodgers, D.W., Gamblin, S.J., Harris, B.A., Ray, S., Culp, J.S., Hellmig, B., Woolf, D.J., Debouck, C., and Harrison, S.C. (1995). The structure of unliganded reverse transcriptase from the human immunodeficiency virus type 1. Proc. Natl. Acad. Sci. USA *92*, 1222–1226.
20. Otwinowski, Z., and Minor, W. (1997). Processing of X-ray diffraction data collected in oscillation mode. In Methods Enzymol. 276A, C.W.J. Carter and R.M. Sweet, eds. (San Diego, CA: Academic Press), 307–326.
21. Hendrickson, W.A. (1976). Radiation damage in protein crystallography. J. Mol. Biol. *106*, 889–893.
22. Henderson, R. (1990). Cryo-protection of protein crystals against radiation damage in electron and x-ray diffraction. Proc. R. Soc. Lond. B Biol. Sci. *241*, 6–8.
23. Teng, T., and Moffat, K. (2000). Primary radiation damage of protein crystals by an intense synchrotron X-ray beam. J. Synchrotron Radiat. *7*, 313–317.
24. Yonath, A., Harms, J., Hansen, H.A., Bashan, A., Schlunzen, F., Levin, I., Koelln, I., Tocilj, A., Agmon, I., Peretz, M., et al. (1998). Crystallographic studies on the ribosome, a large macromolecular assembly exhibiting severe nonisomorphism, extreme beam sensitivity and no internal symmetry. Acta Crystallogr. A *54*, 945–955.
25. Duisenberg, A.J.M., Hooft, R.W.W., Schreurs, A.M.M., and Kroon, J. (2000). J. Appl. Crystallogr. *33*, 893–898.
26. Rodgers, D.W. (1994). Cryocrystallography. Structure *2*, 1135–1140.
27. Glaeser, R., Facciotti, M., Walian, P., Rouhani, S., Holton, J., MacDowell, A., Celestre, R., Cambie, D., and Padmore, H. (2000). Characterization of conditions required for X-Ray diffraction experiments with protein microcrystals. Biophys. J. *78*, 3178–3185.